Applied Catalysis B: Environmental 179 (2015) 128–138

Contents lists available at ScienceDirect

Applied Catalysis B: Environmental

journal homepage: www.elsevier.com/locate/apcatb

Dry reforming of methane over CeO_2 supported Ni, Co and Ni–Co catalysts

Hale Ay, Deniz Üner*

Middle East Technical University, Chemical Engineering, 06800 Ankara, Turkey

ARTICLE INFO

Article history:
Received 11 February 2015
Received in revised form 30 April 2015
Accepted 6 May 2015
Available online 7 May 2015

Keywords:
Dry reforming of methane
Ni
Co
Ni–Co
Ceria supported
Calcination temperature

ABSTRACT

Ceria supported Ni, Co monometallic and Ni–Co bimetallic catalysts were prepared by incipient wetness impregnation method, calcined at two different temperatures (700 °C and 900 °C) and tested for dry reforming of methane reaction at 700 °C. The activities of ceria-based Ni containing catalysts decreased with increasing calcination temperature accompanied by a decrease in coke deposition. While Ni/CeO_2 and $Ni–Co/CeO_2$ catalysts exhibited comparable high activities, Co/CeO_2 catalysts exhibited very low activity. The lower activity of Co/CeO_2 catalyst was attributed to strong metal support interaction (SMSI). The SMSI effect was confirmed with TEM images showing a layer of support coating the metal particles. The diversity of the deposited carbon structures in terms morphology (straight long filaments, highly entangled and curly shaped filaments, filaments with knuckle-like structure and carbon onions) was noted. In addition to the carbon buildup, the deactivation was observed to be due to the loss of active metals in the carbon filaments.

1. Introduction

Syngas (a mixture of carbon monoxide and hydrogen) manufacture is an important step in the production of commodity chemicals, such as ammonia and methanol, as well as liquid fuel production from Fischer–Tropsch synthesis [1–3]. Economics of syngas manufacture depends strongly on the price and availability of the raw material, methane in most situations, which generally determines the economics of the downstream processes [4,5]. The most common processes to convert natural gas into synthesis gas can be listed as steam reforming of methane, partial oxidation of methane and carbon dioxide reforming of methane (or dry reforming of methane) [6]. Carbon dioxide reforming of methane becomes industrially advantageous compared to partial oxidation and steam reforming in synthesis gas production due to the fact that the H_2/CO product ratio in dry reforming is close to one, which is appropriate for further use in the production of oxygenated compounds as well as Fischer–Tropsch synthesis for liquid hydrocarbons production [7]. In addition, dry reforming of methane (DRM) provides the opportunity of using natural gas resources with high carbon dioxide content, avoiding the costly and complicated gas separation process [8]. Dry reforming of methane is also an attractive way of utilizing biogas, a clean and environment friendly fuel that is produced typically from anaerobic degradation of biomass and mainly composed of CO_2 and CH_4 [9]. Dry reforming of methane also eliminates two major greenhouse gases (CO_2 and CH_4) simultaneously while producing valuable feedstock [10].

The catalyst deactivation is the major problem hindering the development of dry reforming of methane. Catalysts can be deactivated due to carbon formation [11–13], sintering at high temperature [14,15] and oxidation of metallic sites [16,17]. Coke formation has been accepted as the primary reason of deactivation [18]. Reversible deactivation due to the carbon build-up can be eradicated by controlled and brief oxidation excursions. The control of temperature during coke oxidation is very important to not to lose active surface areas to sintering of the metal particles. Metal sintering results in irreversible deactivation. On the other hand; carbon buildup in the form of filaments also deactivates the catalysts irreversibly if the growth proceeds by removing the active metal from the support to the tip of the filament.

Although it is known that supported noble metals can provide good catalytic performance in terms of activity, selectivity and resistance to carbon deposition [19,20], Ni based catalysts have been preferred as good replacement due to their comparable catalytic performance, low cost and extensive availability [20,21]. Nevertheless, Ni-based catalysts are well known for their high tendency for carbon deposition [19,21] which can happen by one or more of the following reactions:

$$CH_4 \leftrightarrow C + 2H_2 \quad \Delta H^{\circ}_{298\,K} = 75\,kJ/mol \tag{1}$$

* Corresponding author. Tel.: +90 312 210 4383; fax: +90 312 210 2600.
E-mail address: uner@metu.edu.tr (D. Üner).

http://dx.doi.org/10.1016/j.apcatb.2015.05.013
0926-3373/

$$2CO \leftrightarrow C + CO_2 \quad \Delta H^{\circ}_{298\,K} = -171\,kJ/mol \tag{2}$$

$$CO + H_2 \leftrightarrow C + H_2O \quad \Delta H^{\circ}_{298\,K} = -131\,kJ/mol \tag{3}$$

while, the first reaction is favorable at high temperatures and low pressures, the second and the third one are preferred at low temperatures and high pressures.

In order to decrease the carbon formation tendency of Ni catalysts, several approaches have been proposed: employing appropriate catalyst preparation methods to inhibit coke growth, using metal oxides with strong Lewis basicity as supports or promoters can inhibit coke deposition since Lewis acidity is known to induce coke buildup; addition of a second metal, especially a precious metal, can enhance the transport of hydrogen and/or oxygen between the active catalyst and the support by spillover and can alter the mechanism of coke formation; sulfur passivation is known to block the step edge sites where coke buildup is initiated; introducing steam provides both hydrogen and oxygen to the surface, hence restricting the coke formation steps, changing reaction conditions alters the rates of the coke forming steps [11–13,22,23].

The addition of a second metal is one of the methods applied for dry reforming process with the objective of developing carbon resistance of Ni-based catalysts. There are studies reported on the beneficial effect of noble metal addition, such as Rh [24], Pt [25,26], Pd [27] and Ru [28] to the Ni-based catalyst. From an economic point of view, the addition of a non-noble metal is more preferable. In this respect cobalt is of great interest. But there are significant differences among the results reported in the literature for the effect of Co addition on Ni catalysts for DRM reaction. Xu et al. [9] reported that the catalytic activity of the bimetallic Ni/Co catalysts supported on commercial γ-Al_2O_3 doped with La_2O_3 is closely related to the Ni/Co ratio. While the catalyst having Ni/Co ratio of 7/3 exhibited the highest CH_4 and CO_2 conversion, the catalytic activity decreased considerably if the amount of cobalt was increased further. Bimetallic catalysts having a Ni/Co ratio of 5/5 and 3/7 exhibited lower activity than monometallic Ni catalyst. Takanabe et al. [29] reported that, while, Ni/TiO_2 sample deposited considerable amount of coking particularly at lower temperatures, Co/TiO_2 sample exhibited tendency to be oxidized during dry reforming. On the other hand, the combination of Ni–Co catalyst showed both high catalytic activity and resistance to coke formation during the reaction. The authors suggested that the composition of bimetallic Ni–Co catalyst could be adjusted to alter its catalytic performance for dry reforming of methane. For the Al_2O_3 supported Ni, Co and Ni–Co catalysts, San-Joseí-Alonso et al. [8] showed that the samples containing the highest amount of cobalt (Co(9) and NiCo(1–8)) exhibited the highest activity and stability. However, they produced much higher amount of coke. In their study, carbon deposition increased with increasing Co content, while it decreased with increasing Ni content. Zhang et al. [30] reported that Ni–Co bimetallic catalyst exhibited not only higher activity, but also better stability and carbon resistance compared with the Ni and Co monometallic catalysts. The superior performance of the bimetallic catalyst was attributed to the better metal dispersion, formation of stable solid solutions and strong metal–support interaction.

Cerium oxide and CeO_2-containing materials have been investigated intensively in the field of catalysis for the past several years [31–34]. The broad range applications of ceria is mostly due to its unique redox properties and remarkable oxygen storage capacities [35–37]. Ceria has very good redox properties due to the very quick reduction of Ce^{4+} to Ce^{3+} associated with the creation of oxygen vacancies [38]. It has the ability of releasing oxygen under reducing atmosphere and storing oxygen under oxidizing environment by filling oxygen vacancies [39].

Introducing CeO_2 as an additive promoter to the Ni based catalysts was found to provide considerably higher catalytic activity and resistance to carbon formation in dry reforming of methane reaction [40–42]. There are also studies reporting the use of CeO_2 as support material for Ni catalysts [20,43–45]. On the other hand, CeO_2 supported Co and Ni–Co catalysts have not been investigated in detail. In this study, a comprehensive study on the role of cerium oxide as a support material in Ni/CeO_2, Co/CeO_2 and Ni–Co/CeO_2 was conducted for dry reforming of methane. In order to see the effect of calcination temperature, two different calcination temperatures (700 °C and 900 °C) were used.

2. Experimental

2.1. Preparation of Ni/CeO_2, Co/CeO_2 and Ni–Co/CeO_2 by incipient wetness impregnation method

CeO_2 supported monometallic nickel, monometallic cobalt and bimetallic nickel–cobalt catalysts were prepared by incipient wetness impregnation technique, and calcined at two different temperatures (700 °C and 900 °C). The metal loadings were set at 8 wt% nickel for Ni/CeO_2, 8 wt% cobalt for Co/CeO_2, 8 wt% nickel and 4 wt% cobalt for Ni–Co/CeO_2. Pure CeO_2 support was obtained by calcination of $Ce(C_2H_3O_2)_3{\cdot}1.5H_2O$ at 700 °C for three hours (CeO_2-700) for the catalysts that would be calcined at 700 °C and by calcination of $Ce(C_2H_3O_2)_3{\cdot}1.5H_2O$ at 900 °C for three hours (CeO_2-900) for the catalysts that would be calcined at 900 °C. $Ni(NO_3)_2{\cdot}6H_2O$ (Merck) and $Co(C_2H_3O_2)_2{\cdot}4H_2O$ (Merck) were used as metal sources. The impregnation solution was prepared by dissolving required amount of $Ni(NO_3)_2{\cdot}6H_2O$ and $Co(C_2H_3O_2)_2{\cdot}4H_2O$ in deoinized water. Ni and Co were loaded onto the CeO_2 supports by impregnating them with metal precursor solution to bring about incipient wetness. Ni–Co bimetallic catalysts were prepared by co-impregnation method. The catalysts were dried overnight at room temperature and then at 120 °C for four hours. Finally, the resulting products were calcined at 700 °C as well as 900 °C for 5 h to remove ligands from the nickel and cobalt precursors. The catalysts calcined at 700 °C were denoted as Ni/CeO_2-700, Co/CeO_2-700 and Ni–Co/CeO_2-700. The catalysts calcined at 900 °C were denoted as Ni/CeO_2-900, Co/CeO_2-900 and Ni–Co/CeO_2-900.

2.2. Catalyst characterization

2.2.1. X-Ray diffraction (XRD) analysis

X-ray powder diffraction data were acquired with a Philips model PW1840 X-ray diffractometer using Ni-filtered Cu Kα radiation source (λ = 0.1542 nm) operated at 30 kV and 24 mA. XRD patterns were measured at a scan rate of 0.05°/s.

Some of the XRD patterns were also obtained with Rigaku–Miniflex diffractometer using Cu Kα radiation (wavelength 0.1541 nm, 30 kV, 15 mA).

2.2.2. Surface area, measurements

Micromeritics TriStar II surface area and porosity analyzer were utilized to measure the N_2 adsorption–desorption isotherms of the samples at −196 °C. The samples were degassed for 3 h at 150 °C prior to measurements by means of Micromeritics VacPrep 061 Sample Degas System for removing the moisture and other adsorbed gases from the catalyst surface. The surface area was obtained from multipoint BET (Brunauer–Emmett–Teller) method. The pore volume was estimated from adsorption branch of isotherms by the method of BJH (Barrett–Joyner–Halenda).

2.2.3. Temperature programmed reduction (TPR) analysis

The reducibility of the samples was investigated by H_2 temperature programmed reduction study. TPR experiments were conducted in a ChemiSoft TPx (Micromeritics 2720) instrument. H_2 TPR measurements were set up by heating 100 mg catalyst sample

from room temperature to 900 °C using 25 sccm H_2:Ar (10:90) gas flow at a ramp rate of 10 °C/min.

2.2.4. Thermal gravimetric analysis (TGA)

TGA was carried out to determine the amount of coke deposition on the samples after being used in the CO_2 reforming of CH_4 reaction. The analyses were performed using a Shimadzu DTG 60-H instrument, where each sample was introduced into an alumina microbalance pan that was heated to 900 °C at a rate of 10 °C/min in an oxygen/nitrogen mixture (21:79 vol/vol with a total flow of 69 sccm).

2.2.5. Transmission electron microscopy (TEM)

The morphology of reduced samples was characterized by Jeol 2100F HRTEM machine equipped with Orius SC1000 Model 832 11 Megapixel CCD camera. Before taking the micrographs, the catalysts were dispersed ultrasonically in alcohol and a drop of dispersion was deposited and dried on holey carbon film grid.

The morphology of carbon deposited on the samples after dry reforming of methane reaction was characterized by FEI Tecnai G^2 Spirit Bio (TWIN) HCTEM operated at 120 kV. Before taking the micrographs, the samples were dispersed ultrasonically in alcohol and a drop of dispersion was deposited and dried on a 400 mesh carbon-coated copper grid.

2.2.6. Dry reforming reaction tests

Carbon dioxide reforming of methane reactions was performed in a home built reaction system. The samples in the size range of 0.5–1.0 mm were placed in the center of the 4 mm-i.d. microreactor by quartz wool at both ends. The flow rate of the gases was controlled by using MKS 1179B mass flow controllers. Before the catalytic activity tests, the samples were reduced in 50 sccm H_2:Ar (2:3) by heating from room temperature to 700 °C with 10 °C/min heating rate and kept at this temperature for one hour. 30 sccm pure argon was sent to the reactor for 30 min before switching to the reactant gas mixture. The reactions were carried out at 700 °C with 50 sccm CH_4:CO_2:Ar (1:1:3) gas flow for 5 h. The product gases were sent to a gas chromatograph (HP 5890 Series II) equipped with a thermal conductivity detector and a Carboxen 1010 Plot column by means of a 6 way valve (VICI Valco) with a 100 μL sample loop.

3. Results

3.1. X-ray diffraction (XRD) analysis

XRD was used for the identification of bulk phase feature of the catalysts. Figs. 1 and 2 show the XRD patterns of ceria-based samples calcined at 700 °C and 900 °C, respectively. The pure ceria and the ceria supported catalysts contain face-centered cubic fluorite structure of CeO_2 and show reflections corresponding to (1 1 1), (2 0 0), (2 2 0), (3 1 1), (2 2 2), (4 0 0), (3 3 1) and (4 2 0) planes (JCPDS 34-0394). When calcination temperature increased from 700 °C to 900 °C, a significant increase in the intensity of the peaks was noticed due to the better crystallization of CeO_2.

The particle size of pure-CeO_2-700 and pure-CeO_2-900 supports was estimated as 14.1 nm and 22.9 nm, respectively, by the Scherrer equation using the (1 1 1) reflection at 28.9° in the XRD patterns. The crystal size of ceria was calculated as 15.8 nm, 16.7 nm and 17.4 nm for Ni/CeO_2-700, Co/CeO_2-700 and Ni–Co/CeO_2-700 samples, respectively. The crystal size of ceria was estimated as 24.6 nm, 27.5 nm and 26.7 nm for Ni/CeO_2-900, Co/CeO_2-900 and Ni–Co/CeO_2-900 samples, respectively. As seen, only slight increase were noticed in the CeO_2 crystal size upon the addition of metals.

Ni/CeO_2-700 and Ni/CeO_2-900 exhibit peaks at 37.6°, 43.5° and 63.1–63.2°, corresponding to (1 1 1), (2 0 0) and (2 2 0) planes of NiO, respectively. Co/CeO_2-700 and Co/CeO_2-900 exhibit peaks at

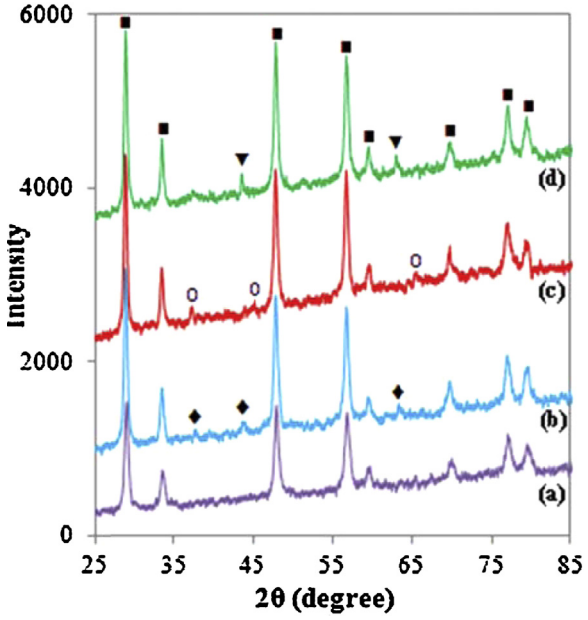

Fig. 1. XRD patterns of catalysts calcined at 700 °C: (a) pure CeO_2-700, (b) Ni/CeO_2-700 (c) Co/CeO_2-700, and (d) Ni–Co/CeO_2-700, ■ CeO_2, ♦ NiO, Co_3O_4,▼$Ni_xCo_{1-x}O$.

37.1°, 45.0–45.1° and 65.4–65.5°, corresponding to (3 1 1), (4 0 0) and (4 4 0) planes of Co_3O_4, respectively.

There are new diffraction peaks observed in the XRD patterns of Ni–Co/CeO_2-700 and Ni–Co/CeO_2-900. The first one is at 43.3°, whose position is lower than the nearest NiO (2 0 0) and Co_3O_4 (4 0 0). The second one is at 62.8°, the position of which is lower than the nearest NiO (2 2 0) and Co_3O_4 (4 4 0). As a result, these two peaks were attributed to the formation of a solid solution $Ni_xCo_{1-x}O$ [46]. Ni–Co/CeO_2-700 and Ni–Co/CeO_2-900 also exhibit a weak diffraction peak at 37.2–37.3° between NiO (1 1 1) and Co_3O_4 (3 1 1), indicating the formation of a nickel–cobalt mixed oxide.

In Fig. 3, the XRD patterns of the reduced catalysts were presented along with the XRD patterns of the spent catalysts. While the reduced monometallic nickel catalysts exhibited (1 1 1) peak of Ni^0,

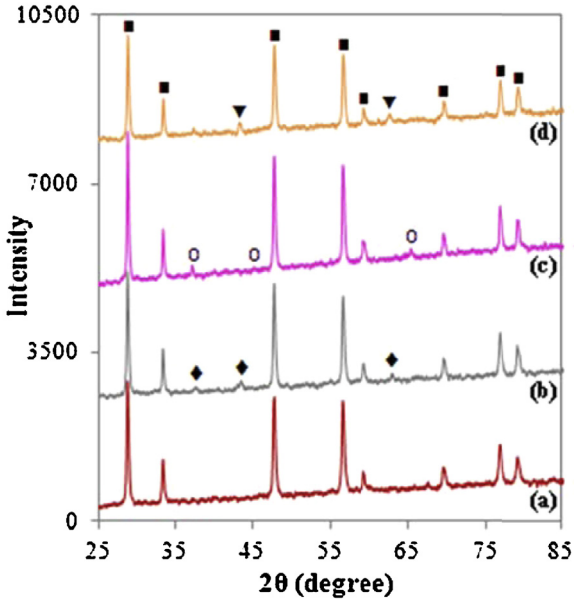

Fig. 2. XRD patterns of catalysts calcined at 900 °C: (a) pure CeO_2-900, (b) Ni/CeO_2-900 (c) Co/CeO_2-900, and (d) Ni–Co/CeO_2-900, ■ CeO_2, ♦ NiO, Co_3O_4, ▼$Ni_xCo_{1-x}O$.

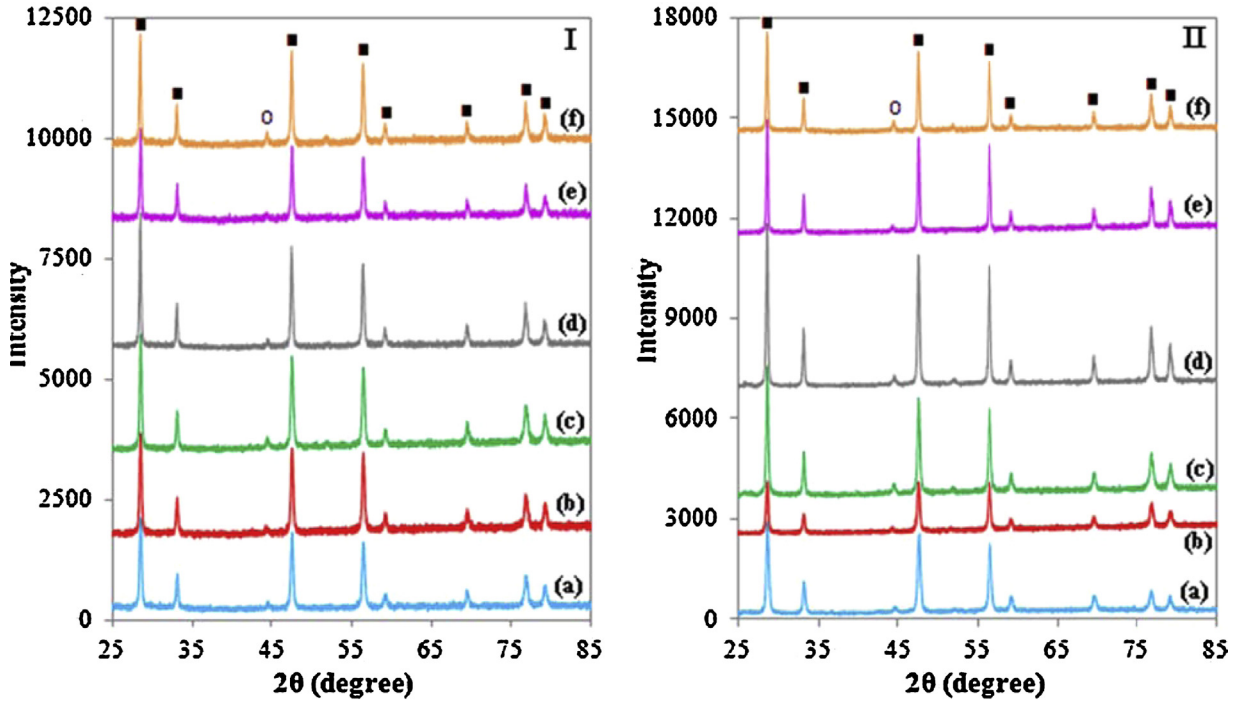

Fig. 3. XRD patterns of reduced catalysts (I) and spent catalysts (II), (a) Ni/CeO_2-700, (b) Co/CeO_2-700, (c) $Ni–Co/CeO_2$-700, (d) Ni/CeO_2-900, (e) Co/CeO_2-900, and (f) $Ni–Co/CeO_2$-900, ■ CeO_2, ○ Ni° or Co°.

the reduced monometallic cobalt catalysts exhibited (1 1 1) peak of Co^0. Reduced bimetallic catalysts exhibited a peak whose position is between Co^0 (1 1 1) and Ni^0 (1 1 1), confirming the formation of a Ni–Co alloy after reduction. The reduced catalyst pattern is repeated in the spent catalyst XRD as well, indicating that the catalyst maintained its reduced state during and after the reaction.

3.2. Textural properties

The textural properties of the samples calcined at 700 °C and 900 °C were investigated by nitrogen adsorption–desorption measurements (Table 1). The surface area of the pure CeO_2 obtained by calcination of cerium acetate at 900 °C was much lower than the one obtained by calcination of cerium acetate at 700 °C. The loss of surface area upon thermal treatment at higher temperature was due to gradual sintering and crystallite growth [47]. When Ni, Co or Ni–Co was added to the support and calcined again, the surface area and the total pore volume decreased significantly. The pore volume decrease in accordance with the surface area decrease of the metal loaded samples suggests that the metals are deposited inside the pores of CeO_2.

3.3. Temperature programmed reduction (TPR) analysis

The reducibility of the samples was investigated by TPR. Generally, there are three main reduction peaks which were attributed to the reduction of metal oxides, surface ceria and bulk ceria. While the broad reduction peaks in the temperature range of 350–550 °C were assigned to the surface reduction of ceria, the peaks appearing after 650 °C were ascribed to the bulk reduction of ceria [48,49] (Fig. 4).

For nickel loaded samples, the smallest peak seen at 182 °C for Ni/CeO_2-700 and at 174 °C for Ni/CeO_2-900 can be attributed to the reduction of adsorbed oxygen which can be reduced by hydrogen at low temperatures [50]. It was shown in literature that the

Table 1
Textural properties of the samples.

Catalyst	BET surface area (m^2/g)	Pore volume (cm^3/g)
Pure CeO_2-700	40.5	0.16
Ni/CeO_2-700	23.8	0.12
Co/CeO_2-700	18.9	0.10
$Ni–Co/CeO_2$-700	18.3	0.10
Pure CeO_2-900	14.4	0.09
Ni/CeO_2-900	7.9	0.04
Co/CeO_2-900	4.3	0.02
$Ni–Co/CeO_2$-900	5.8	0.02

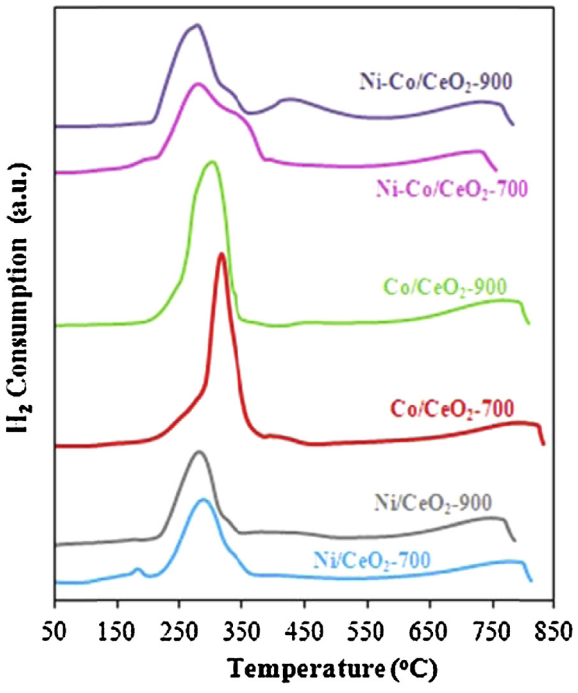

Fig. 4. TPR profiles of catalysts.

reduction of pure NiO consists of two reduction peaks corresponding to the stepwise reduction of NiO: $NiO \rightarrow Ni^{\delta+} \rightarrow Ni^0$ [50]. The main reduction peak seen at 287 °C for Ni/CeO_2-700 and at 279 °C for Ni/CeO_2-900 was attributed to the reduction of NiO to $Ni^{\delta+}$. The shoulder observed at 323 °C for Ni/CeO_2-700 and at 316 °C for Ni/CeO_2-900 was attributed to the reduction of $Ni^{\delta+} \rightarrow Ni^0$.

According to the literature, the reduction of pure Co_3O_4 takes place as a two-step reduction process via $Co_3O_4 \rightarrow CoO \rightarrow Co^\circ$ [51,52]. While the shoulder observed at 284 °C for Co/CeO_2-700 and 251 °C for Co/CeO_2-900 was attributed to the reduction of $Co_3O_4 \rightarrow CoO$, the main peak seen at 315 °C for Co/CeO_2-700 and 301 °C for Co/CeO_2-900 was attributed to the reduction of $CoO \rightarrow Co^\circ$.

Bimetallic samples exhibited a complex reduction profile. The main reductions were observed at 279 °C for Ni–Co/CeO_2-700 and 278 °C for Ni–Co/CeO_2-900, and they were both lower than the main reduction temperatures of monometallic catalyst, which may be attributed to the formation of nickel–cobalt alloy. The other peaks can be due to the overlapped reduction peaks of both nickel and cobalt. They exhibited a small temperature reduction peak which is close to the observed in the monometallic nickel samples. The shoulders observed at 320 °C for Ni–Co/CeO_2-700 and 318 °C for Ni–Co/CeO_2-900 were again very close to the ones observed in monometallic nickel samples which were attributed to the reduction of $Ni^{\delta+} \rightarrow Ni^0$.

3.4. Dry reforming reaction results

The time dependent CH_4 and CO_2 conversion over the catalysts calcined at 700 °C are given in Fig. 5. Ni/CeO_2-700 and Ni–Co/CeO_2-700 provided comparable high activities. Although showing a slight decrease in activity in the first period of reaction, both of them preserved their performance up to the end of the reaction.

Co/CeO_2-700 exhibited very low activity compared to Ni/CeO_2-700 and Ni–Co/CeO_2-700. There are some studies in literature making the same conclusion over different supports [29,53]. In this study, both CH_4 conversion and CO_2 conversion of Co/CeO_2-700 exhibited a decreasing trend as the reaction proceeded (Fig. 5). While the initial CH_4 conversion of Co/CeO_2-700 was 16%, it decreased to 6% after 5 h of reaction. Likewise, the initial CO_2 conversion of Co/CeO_2-700 was 25% and fell down to 7% after 5 h reaction period.

In order to understand the effect of calcination temperature, the activity of the catalysts calcined at 900 °C were also investigated for dry reforming of methane. CH_4 and CO_2 conversions versus time on stream over the catalysts calcined at 900 °C are given in Fig. 6. When Figs. 5 and 6 are compared to each other, it is seen that conversion of CH_4 and CO_2 decreased with the increase of calcination temperature from 700 °C to 900 °C. The initial deactivation was more severe for the catalysts calcined at 900 °C.

The time dependent H_2 and CO yield of the catalysts calcined at 700 °C and 900 °C are given in Figs. 7 and 8, respectively. The catalysts calcined at 700 °C exhibited better performance in terms of H_2 and CO production than the ones calcined at 900 °C. CO yield was higher than H_2 yield for all the catalysts due to the reverse water–gas shift reaction, , supported by higher CO2 conversions than CH_4. Since CO yield was higher than H_2 yield, the H_2/CO ratio was lower than 1.0 for all the catalysts examined.

3.5. Thermal gravimetric analysis (TGA)

The amount of carbon deposited on the samples after being used in CO_2 reforming of CH_4 was determined by TGA. The weight losses as a result of combustion of the carbon deposited on the spent catalysts are shown in Fig. 9. The carbon deposition over the Ni and Ni–Co catalysts decreased with an increase of calcination temperature from 700 °C to 900 °C (from 20.7 wt% to 17.5 wt% for Ni catalyst, from 26.1 wt% to 11.5 wt% for Ni–Co catalyst) which was in accordance with the lower activity of the catalysts prepared by calcination at 900 °C. The derivative of the TGA curves shown in Fig. 9 are presented in Fig. 10. All of the catalysts exhibited an oxidation peak at around 510–560 °C. The only distinctive feature observed in these figures is the sharp peak corresponding to Ni–Co/CeO_2-700 giving a peak oxidation rate at about 470 °C.

3.6. Transmission electron microscopy (TEM)

The morphology of fresh catalysts in their reduced state was studied by HRTEM and shown in Fig. 11 for Co/CeO_2-700 (a and b) and Ni–Co/CeO_2-700 (c and d) catalysts. From Fig. 11, a thin layer coating the metal particles and the support is clearly seen. This layer is interpreted as partially reduced ceria indicating strong metal support interaction (SMSI) and will be further discussed in the next section.

The morphology of carbon deposited on the samples after the reaction were analyzed by HCTEM and shown in Fig. 12 for Ni/CeO_2-700 (a and b) and Ni–Co/CeO_2-700 (c and d) catalysts. Abundant filamentous carbon growth with varying dimensions is seen. There are both thin-walled tubes with wide inner channels and thick-walled tubes with narrow inner channels. While some of them are straight long filaments approaching several micrometers, most of them are curly shaped and highly entangled. Some of the carbon filaments have a knuckle-like structure with irregular width.

4. Discussion

In this study, we have observed significant amount of coke deposition during dry reforming of methane over all of the catalysts that has demonstrated considerable activity. In this section, we will present our interpretations of the data and their comparison to the literature wherever possible. We will further elaborate on the absence of activity over the Co based catalysts.

XRD characterization of the monometallic catalysts revealed NiO and Co_3O_4 after calcinations. (Figs. 1 and 2). We particularly paid attention to the peaks for mixed oxides and alloys. Ni–Co/CeO_2-700 and Ni–Co/CeO_2-900 exhibit new diffraction peaks than the ones observed in monometallic catalysts. The first one is positioned at 43.3°, lower than the nearest NiO (2 0 0) and Co_3O_4 (4 0 0). The second one is located at 62.8°, lower than the nearest NiO (2 2 0) and Co_3O_4 (4 4 0). High temperature calcination can lead to spinel formation for the samples containing Ni and Co [30,54–56]. But when these peaks are compared to characteristic peaks of $NiCo_2O_4$ (JCPDS 73-1702), it was concluded that the peak positioned at 43.3° cannot be indexed to the nearest $NiCo_2O_4$ (2 2 2) and $NiCo_2O_4$ (4 0 0). It was also concluded that the peak positioned at 62.8° cannot be indexed to the nearest $NiCo_2O_4$ (5 1 1) and $NiCo_2O_4$ (4 4 0). As a result, these two peaks were attributed to the formation of a solid solution $Ni_xCo_{1-x}O$ [46].

After the reduction, metallic forms of Ni and Co were identified for monometallic catalysts. The XRD results exhibited only one peak for the metallic phase for bimetallic catalysts, the position of which was identified between the metallic Co and Ni, indicating a definitive evidence for alloy formation between Ni and Co during reduction Fig. 3.

The reducibility of the catalysts was investigated through TPR measurements (Fig. 4). The TPR signals were not calibrated, therefore, a quantitative comparison is not possible. However, a qualitative comparison will be provided below. The areas under the TPR peaks up to 550 °C were determined as area units per gram of catalyst and are presented in Table 2. The H_2 consumption related with the bulk CeO_2 were not considered in area determinations.

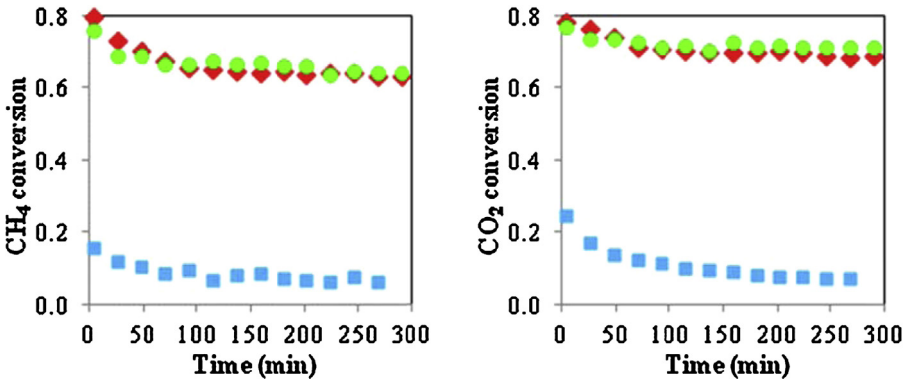

Fig. 5. Comparison of CH_4 and CO_2 conversion versus time on stream over the catalysts calcined at 700 °C, Ni/CeO_2-700 ◆, Co/CeO_2-700 ■, $Ni–Co/CeO_2$-700 ●. Reaction conditions: 700 °C, 1 atm, 50 sccm feed with $CH_4/CO_2/Ar = 1/1/3$.

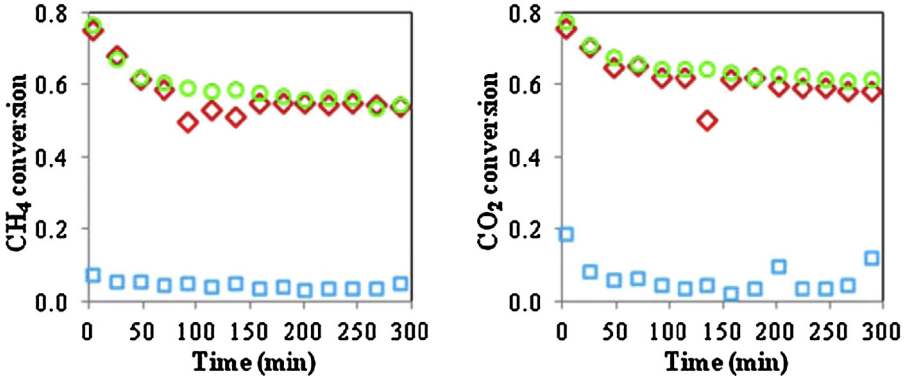

Fig. 6. Comparison of CH_4 and CO_2 conversion versus time on stream over the catalysts calcined at 900 °C, Ni/CeO_2-900 ◇, Co/CeO_2-900 □, $Ni–Co/CeO_2$-900 ○. Reaction conditions: 700 °C, 1 atm, 50 sccm feed with $CH_4/CO_2/Ar = 1/1/3$.

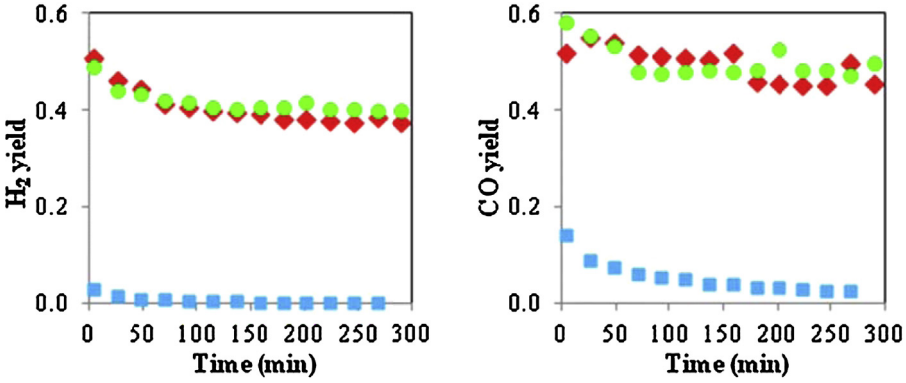

Fig. 7. Comparison of H_2 and CO yield versus time on stream over the catalysts calcined at 700 °C, Ni/CeO_2-700 ◆, Co/CeO_2-700 ■, $Ni–Co/CeO_2$-700 ●. Reaction conditions: 700 °C, 1 atm, 50 sccm feed with $CH_4/CO_2/Ar = 1/1/3$.

Table 2
Comparison of the experimental H_2 Consumption from TPR relative to complete reduction from NiO and/or Co_3O_4.

	Measured H_2 consumption (area/g catalyst)		Expected H_2 consumption (mmol/g)	Normalized H_2 consumption with respect to Ni/CeO_2		
	Calcined at 700 °C	Calcined at 900 °C		Calcined at 700 °C	Calcined at 900 °C	Expected H_2 consumption
Ni/CeO_2	5.8	5.5	1.4	1.00	1.00	1.00
Co/CeO_2	7.2	7.9	1.8	1.24	1.44	1.29
$Ni–Co/CeO_2$	8.0	8.7	2.3	1.38	1.58	1.64

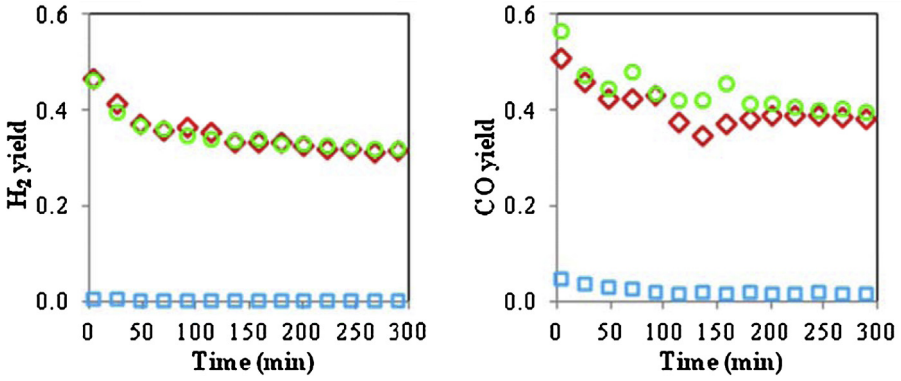

Fig. 8. Comparison of H_2 and CO yield versus time on stream over the catalysts calcined at 900 °C, Ni/CeO_2-900, Co/CeO_2-900, Ni–Co/CeO_2-900. Reaction conditions: 700 °C, 1 atm, 50 sccm feed with $CH_4/CO_2/Ar = 1/1/3$.

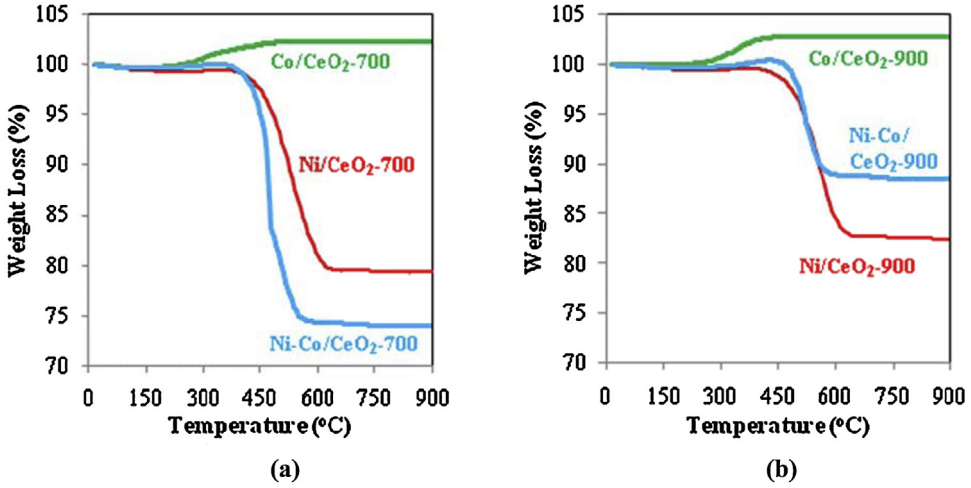

Fig. 9. TGA curves in air atmosphere after being used in reaction at 700 °C for 5 h for the catalysts calcined at (a) 700 °C and (b) 900 °C.

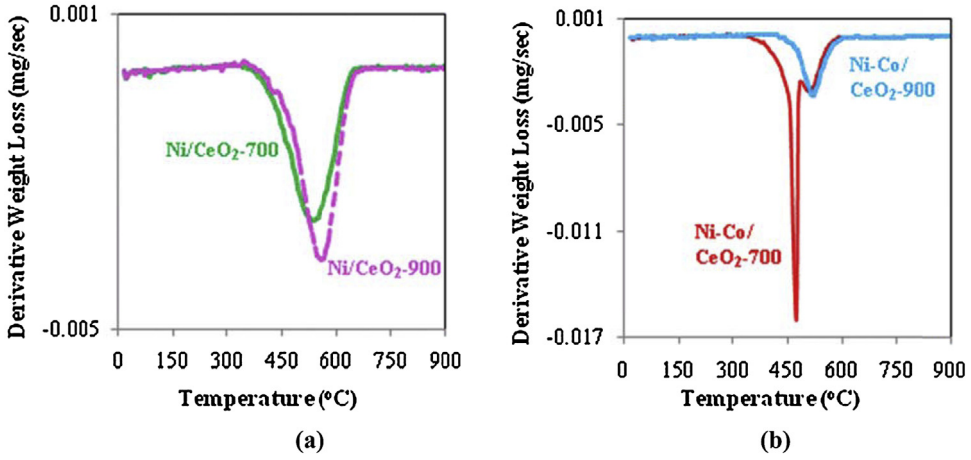

Fig. 10. Derivative weight losses of the catalysts after being used in the reaction at 700 °C for 5 h (a) Ni/CeO_2 and (b) Ni–Co/CeO_2.

In addition, theoretical amount of H_2 demanded was calculated by assuming complete reduction of NiO to Ni^0 for Ni/CeO_2 samples and complete reduction of Co_3O_4 to Co^0 for Co/CeO_2 samples. For Ni–Co/CeO_2 samples, complete reduction of both NiO and Co_3O_4 was assumed by taking into consideration their metal loadings. These values are also presented in Table 2. The comparison between the experimental data and the theoretical values could only be performed as the relative change. This change was based on the values of Ni/CeO_2 and also given in Table 2. It is seen that the H_2 consumption for the reduction of catalysts were consistent with the expected values. The deviations were attributed to the surface reduction of CeO_2 and hydrogen spillover to the CeO_2 support.

The initial deactivation observed in our catalysts (Figs. 5–8) is not as severe as some of the reported values in the literature. For example, Wang and Lu [42] reported that an initial quick (non-linear) deactivation took place over Ni/CeO_2 catalyst at 700 °C.

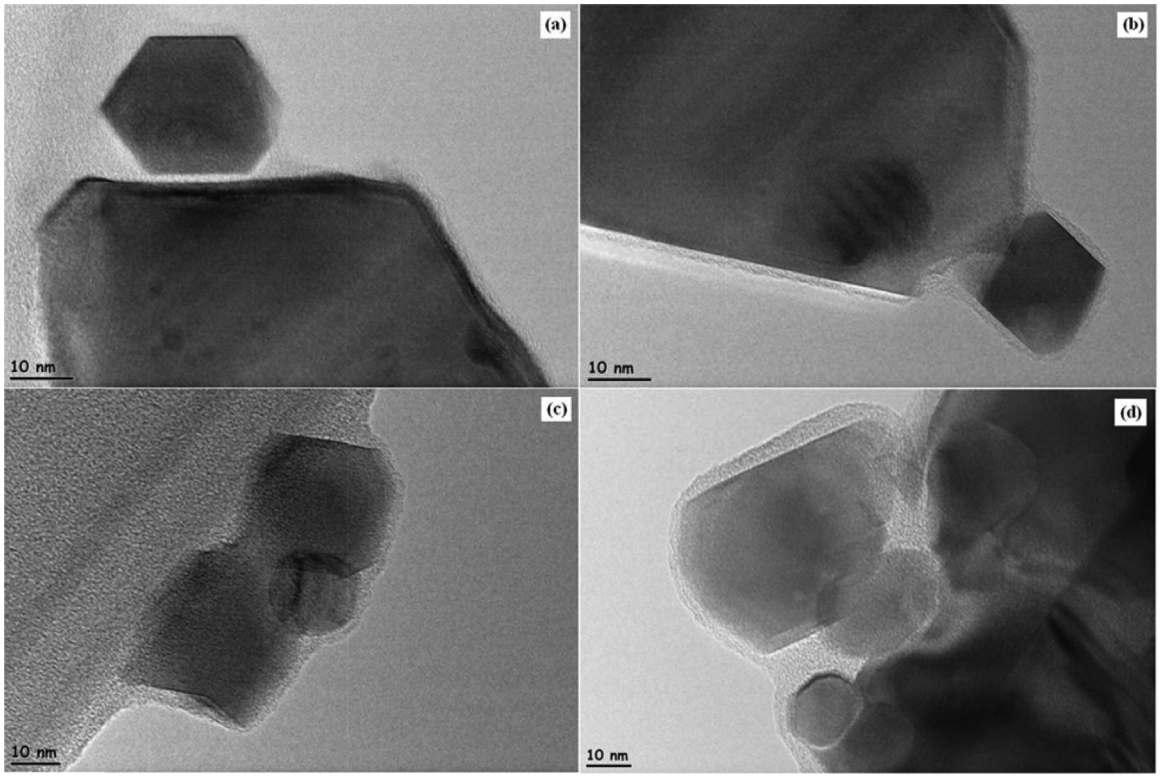

Fig. 11. HRTEM of reduced (a and b) Co/CeO_2-700 and (c and d) $Ni–Co/CeO_2$-700 catalysts showing the decoration of metal particles with a thin layer of support, indicating SMSI effect.

After 5 h, a linear deactivation rate was seen. Asami et al. [43] also observed such deactivation over CeO_2 supported Ni catalyst at 700 °C; the initial conversion of CH_4 was 30%, and it fell rapidly to only several percentage points within 2–3 h on stream. On the other hand, Gonzalez-DelaCruz et al. [57] observed a gradually decreasing trend over Ni/CeO_2 catalyst at 750 °C. While the CH_4 conversion was 75% initially, it decreased slowly to 65% after approximately 500 min on reaction and pretty much stable up to 1000 min. Du et al. [20] did not observe an initial deactivation, but a slightly decreasing activity over nickel catalysts supported on CeO_2 nanorods (NR) and CeO_2 nanopolyhedra (NP) during 30 h on stream. The CH_4 conversion was reduced by 21.9% and 26.2% for the Ni/CeO_2-NR and Ni/CeO_2-NP, respectively, while the CO_2 conversion experienced deactivation of 12.1% and 15.1% for the Ni/CeO_2-NR and Ni/CeO_2-NP, respectively.

Co/CeO_2 catalyts exhibited very low activity compared to Ni/CeO_2 and $Ni–Co/CeO_2$ samples (Figs. 5–8). The surprising low activity observed in Co/CeO_2 catalysts could be due to formation of a perovskite phase [58], oxidation of metal [17] and less activity of Co metal compared to Ni [9]. The formation of perovskite and metal oxidation possibilities was eliminated by post reaction XRD patterns (Fig. 3) which showed that cobalt maintains its metallic phase even after the reaction tests.

On the contrary, HRTEM images shown in Fig. 11 provided clear evidence for strong metal–support interaction effect. The strong metal–support interaction phenomenon occurs upon high temperature reduction. Thermal and chemical effects during high temperature reduction induces migration of the partially reduced support on the metal surface. As a result, the metal particles are partly covered by a thin layer of the reduced support, thus, blocking the chemisorption active centers at the metal surface. These arguments were supported by a number of experimental techniques, and particularly HRTEM [59,60]. We have also observed a thin layer covering, especially Co monometallic and bimetallic Co-Ni catalysts as shown in Fig. 11. Despite significant effort that we spent to measure hydrogen chemisorption in an adsorption calorimeter available in our laboratory [61], no evidence for hydrogen chemisorption over these catalysts could be obtained, supporting our SMSI arguments. The strong metal–support interaction was reported to be a disadvantage for bulk ceria-supported nickel catalysts in dry reforming of methane reaction reducing the catalytic activity [11,42,62]. Wang and Lu [42] reported that CeO_2 exhibited different behaviors as a promoter or support. CeO_2 was shown to provide positive effect on catalytic activity, stability, and carbon suppression when used as a promoter in Ni/Al_2O_3 [42]. On the other hand, ceria as support for Ni catalysts produced strong metal–support interaction which reduced the catalytic activity [42].

There are also some studies in literature regarding SMSI as an advantage over ceria supported materials for dry reforming of methane. Gonzalez-DelaCruz et al. [57] noticed that nickel particles in a Ni/CeO_2 catalyst underwent unexpected modifications in their size and morphology under dry reforming of methane conditions. They were flattened and strongly stabilized on the partially reduced CeO_2 surface. The authors suggested that these morphology changes reflected a kind of SMSI and could account for the higher stability observed for CO_2 reforming of CH_4 reaction. In their study, Du et al. [20] compared the catalytic activity and coke resistance of Ni/CeO_2 nanorods (NR) and nanopolyhedra (NP). The Ni/CeO_2-NR exhibited much better catalytic activity and coke resistance than the Ni/CeO_2-NP. The HRTEM showed that CeO_2-NR had unusually reactive (1 1 0) and (1 0 0) planes, while Ni/CeO_2-NP had stable (1 1 1) plane. The (1 1 0) and (1 0 0) planes exhibited remarkable superiority for the anchoring of nickel particles, suggesting SMSI. They concluded that SMSI effect was helpful in preventing sintering of particles, which was beneficial for the reduction of deactivation.

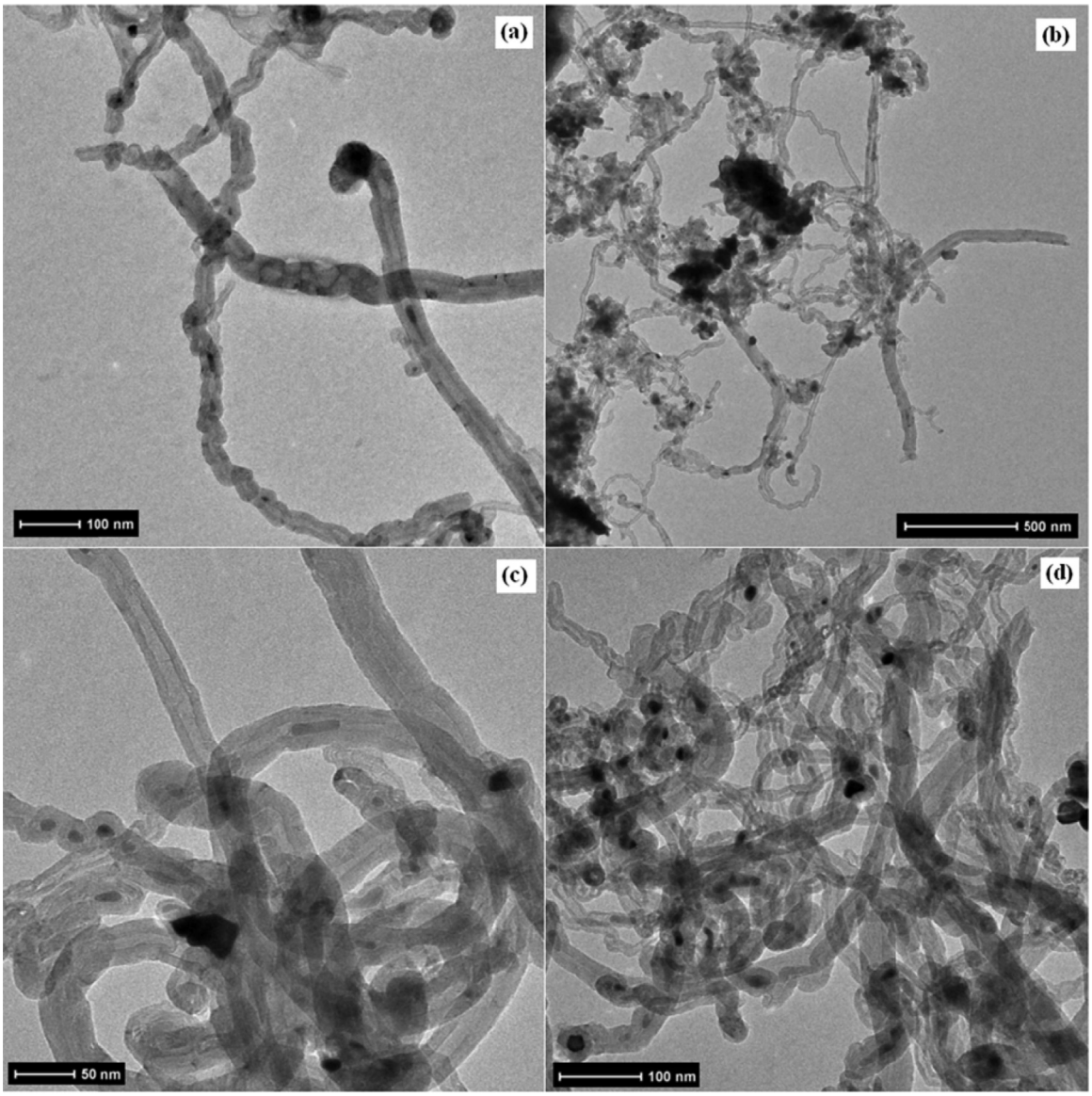

Fig. 12. HCTEM of (a and b) Ni/CeO_2-700 and (c and d) Ni–Co/CeO_2-700 catalysts after being used in reaction at 700 °C for 5 h.

In this study, no beneficial effect was observed on CH_4 and CO_2 conversion by incorporation of Co to the Ni-based ceria catalyst. It must be noted that an optimum Co/Ni ratio was reported to improve the activity of Ni catalyst toward DRM [9,63]. Unfortunately, we did not do such an exploration and the selected Co loading may be outside the optimum level.

The deposited coke amounts and their oxidation behaviors were characterized by TGA under air. It was observed that higher amount of coke deposited on Ni–Co/CeO_2 when the calcination was done at 700 °C. On the other hand, deposited amount of coke did not change significantly on Ni/CeO_2 upon the change in the calcination temperature. No carbon was deposited on monometallic Co catalysts which could be ascribed to its poor activity for dry reforming of methane reaction. On the contrary, a slight weight gain was seen over monometallic Co catalysts which might be due to the oxidation of metallic cobalt. The active sites of Co toward DRM are also active for coke deposition. The absence of activity and the absence of coke deposition correlate very well. The shift in coke oxidation peak maxima from 535 °C to 560 °C for Ni/CeO_2 and from 510 °C to 525 °C for Ni–Co/CeO_2 with the increase of calcination temperature from 700 °C to 900 °C could be interpreted as the formation of more stable carbons. When cobalt is added to the Ni-based catalysts, the oxidation peak decreased from 535 °C to 510 °C for the catalysts calcined at 700 °C and from 560 °C to 525 °C for the catalysts calcined at 900 °C. It means that addition of cobalt to the Ni-based catalysts resulted in less stable carbon formation.

The derivative weight loss of the spent catalysts was plotted to differentiate the different types of carbon deposited during the reaction (Fig. 10). Two distinctive peaks were observed for Ni–Co/CeO_2-700 indicating two different types of carbon formation; the first type can be oxidized at around 470 °C and the second type can be oxidized at around 510 °C. On the other hand, Ni/CeO_2-700, Ni/CeO_2-900 and Ni–Co/CeO_2-900 had only one peak indicating the formation of only one kind of carbon formation which can be oxidized at around 535 °C, 560 °C and 525 °C, respectively. It is generally accepted that amorphous carbon decompose at the lowest temperatures, followed by single walled carbon nanotubes, then multi-walled carbon nanotubes and graphite [64]. The thermogravimetric analysis conducted by Bom et al. showed that graphite has a higher thermal stability than multi-walled carbon nanotubes and, hence, oxidize at higher temperatures [65]. The oxidation temperatures are typically in the range of 200–300 °C for

amorphous carbon, 350–500 °C for single walled carbon nanotubes and 400–650 °C for multi-walled carbon nanotubes [64]. The oxidation peaks which were observed after 500 °C were all attributed to the burning of multi-walled carbon nanotubes. In order to reveal the morphology of deposited carbon and especially for the one that oxidized at 470 °C, TEM images were used (Fig. 12), albeit not a clear differentiation was possible. The differences observed in the oxidation temperature of carbon nanotubes depend on several parameters, such as diameter of the tubes [66,67], length of the tubes [68], percentage of metal loading used in the production of the nanotube [69,70]. The diversity of the deposited carbon structures in terms morphology (straight long filaments, highly entangled and curly shaped filaments, filaments with knuckle-like structure and carbon onions) can be another reason for the presence of two distinctive peaks in the derivative weight loss of spent Ni–Co/CeO_2-700.

The position of the metal particle is very essential for the stability of the catalyst [8]. It may either stay at the top of the filament or may be enclosed within the filament. If the metal particle is at the top of the filament, it is reachable to the reactants and, therefore, it preserves the catalytic activity for some time. On the other hand, the catalytic activity is lost when the metal particle is embedded due to the fact that the reactants cannot access to the active metal sites anymore [8]. While some metal particles are seen at the tip of the filaments, some of them are encapsulated within carbon resulting in the deactivation of the catalyst. It must be noted here that once the metals are detached from the support in or on the carbon filaments, the regeneration is not possible. It is very important to elaborate on the reaction engineering and chemical thermodynamic aspects of this reaction system which operates at the extreme temperatures leading to severe heat and mass transfer limitations.

5. Conclusions

Dry reforming of methane was carried out over CeO_2 supported Ni, Co monometallic and Ni–Co bimetallic catalysts which were prepared by incipient wetness impregnation method at two different calcination temperatures (700 °C and 900 °C). The activities of the catalyst decreased with an increase in calcination temperature. Both Ni/CeO_2 and Ni–Co/CeO_2 catalysts exhibited comparable high activities at both calcination temperatures indicating that Co did not influence the performance of Ni. On the other hand, Co/CeO_2 catalysts exhibited much lower performance than Ni/CeO_2 and Ni–Co/CeO_2 catalysts due to the SMSI. Based on TEM and reaction data, we conclude that Co/CeO_2 system is more susceptible to the SMSI effect than Ni/CeO_2. While no carbon formation was observed over Co/CeO_2 due its poor catalytic activity, the carbon deposition over the Ni/CeO_2 and Ni–Co/CeO_2 catalysts decreased with increasing calcination temperature which was more pronounced on Ni-Co/CeO_2.

Acknowledgement

The authors acknowledge The Scientific and Technological Research Council of Turkey (TUBITAK) for financial support (Project code: 112M561).

References

[1] E.V. Kondratenko, M. Baerns, Synthesis gas generation by heterogeneous catalysis, in: I. Horvath (Ed.), Encyclopedia of Catalysis, vol. 6, John Wiley and Sons, New York, 2003, pp. 424–456.
[2] A.P.E. York, T.C. Xiao, M.L.H. Green, J.B. Claridge, Methane oxyforming for synthesis gas production, Catal. Rev. 49 (4) (2007) 511–560.
[3] X.E. Tsipouriari, V.A. Verykios, Carbon and oxygen reaction pathways of CO_2 reforming of methane over Ni/La_2O_3 and Ni/Al_2O_3 catalysts studied by isotopic tracing techniques, J. Catal. 187 (1999) 85–94.
[4] A.S.K. Raju, C.S. Park, J.M. Norbeck, Synthesis gas production using steam hydrogasification and steam reforming, Fuel Process. Technol. 90 (2) (2009) 330–336.
[5] B. Fidalgo, J.A. Menéndez, Syngas production by CO_2 reforming of CH_4 under microwave heating – challenges and opportunities, in: A. Indarto, J. Palgunadi (Eds.), Syngas: Production, Applications and Environmental Impact, Nova Science Publishers Inc., New York, 2013, pp. 121–149.
[6] L.A. Arkatova, The deposition of coke during carbon dioxide reforming of methane over intermetallides, Catal. Today 157 (2010) 170–176.
[7] Ş. Özkara-Aydınoğlu, E. Özensoy, A.E. Aksoylu, The effect of impregnation strategy on methane dry reforming activity of Ce promoted Pt/ZrO_2, Int. J. Hydrogen Energy 34 (2009) 9711–9722.
[8] D. San-José-Alanso, J. Juan-Juan, M.J. Illán-Gómez, M.C. Román-Martínez, Ni, Co and bimetallic Ni–Co catalysts for the dry reforming of methane, Appl. Catal. A: Gen. 371 (2009) 54–59.
[9] J. Xu, W. Zhou, Z. Li, J. Wang, J. Ma, Biogas reforming for hydrogen production over nickel and cobalt bimetallic catalysts, Int. J. Hydrogen Energy 34 (2009) 6646–6654.
[10] Y. Qu, A.M. Sutherland, T. Guo, Carbon dioxide reforming of methane by Ni/Co nanoparticle catalysts immobilized on single-walled carbon nanotubes, Energy Fuels 22 (2008) 2183–2187.
[11] C. Papadopoulou, H. Matralis, X. Verykios, Utilization of biogas as a renewable carbon source: dry reforming of methane, in: L. Guczi, A. Erdôhelyi (Eds.), Catalysis for Alternative Energy Generation, Springer Science + Business Media, New York, 2012, pp. 57–127.
[12] M.C.J. Bradford, M.A. Vannice, CO_2 reforming of CH_4, Catal. Rev.: Sci. Eng. 41 (1) (1999) 1–42.
[13] J.R. Rostrup-Neilsen, J.H. Bak-Hansen, CO_2-reforming of methane over transition metals, J. Catal. 144 (1993) 38–49.
[14] Z.L. Zhang, V.A. Tsipouriari, A.M. Efstathiou, X.E. Verykios, Reforming of methane with carbon dioxide to synthesis gas over supported rhodium catalysts. I. Effects of support and metal crystallite size on reaction activity and deactivation characteristics, J. Catal. 158 (1996) 51–63.
[15] J. Guo, H. Lou, H. Zhao, D. Chai, X. Zheng, Dry reforming of methane over nickel catalysts supported on magnesium aluminate spinels, Appl. Catal. A: Gen. 273 (2004) 75–82.
[16] K. Nagaoka, K. Takanabe, K.I. Aika, Modification of Co/TiO_2 for dry reforming of methane at 2 MPa by Pt, Ru or Ni, Appl. Catal. A: Gen. 268 (2004) 151–158.
[17] H.Y. Ruckenstein, E. Wang, Carbon deposition and catalytic deactivation during CO_2 reforming of CH_4 over Co/γ-Al_2O_3 catalysts, J. Catal. 205 (2002) 289–293.
[18] K. Nagaoka, K. Seshan, K.I. Lercher, J.A. Aika, Activation mechanism of methane-derived coke (CH_x) by CO_2 during dry reforming of methane – comparison for Pt/Al_2O_3 and Pt/ZrO_2, Catal. Lett. 70 (2000) 109–116.
[19] Z.F. Yan, R.G. Ding, L.H. Song, L. Qian, Mechanistic study of carbon dioxide reforming with methane over supported nickel catalysts, Energy Fuels 12 (6) (1998) 1114–1120.
[20] X. Du, D. Zhang, L. Shi, R. Gao, J. Zhang, Morphology dependence of catalytic properties of Ni/CeO_2 nanostructures for carbon dioxide reforming of methane, J. Phys. Chem. C 116 (2012) 10009–10016.
[21] D. Liu, X.Y. Quek, W.N.E. Cheo, R. Lau, A. Borgna, Y. Yang, MCM-41 supported nickel-based bimetallic catalysts with superior stability during carbon dioxide reforming of methane: effect of strong metal–support interaction, J. Catal. 266 (2009) 380–390.
[22] R. Navarro, B. Pawelec, M.C. Alvarez-Galván, R. Guil-Lopez, S. Al-Sayari, J.L.G. Fierro, Renewable syngas production via dry reforming of methane, in: M. De Falco, G. Iaquaniello, G. Centi (Eds.), CO_2: A Valuable Source of Carbon, Green Energy and Technology, Springer–Verlag, London, 2013, pp. 45–66.
[23] N.A. Pechimuthu, S.C. Pant, K.K. Dhingra, Deactivation studies over Ni–K/CeO_2–Al_2O_3 catalyst for dry reforming of methane, Ind. Eng. Chem. Res. 46 (2007) 1731–1736.
[24] Z. Hou, P. Chen, H. Fang, X. Zheng, T. Yashima, Production of synthesis gas via methane reforming with CO_2 on noble metals and small amount of noble-(Rh-) promoted Ni catalysts, Int. J. Hydrogen Energy 31 (2006) 555–561.
[25] M. García-Diéguez, I.S. Pieta, M.C. Herrera, M.A. Larrubia, L.J. Alemany, Improved Pt–Ni nanocatalysts for dry reforming of methane, Appl. Catal. A: Gen. 377 (2010) 191–199.
[26] D. Liua, W.N.E. Cheo, Y.W.Y. Lim, A. Borgna, R. Lau, Y. Yang, A comparative study on catalyst deactivation of nickel and cobalt incorporated MCM-41 catalysts modified by platinum in methane reforming with carbon dioxide, Catal. Today 154 (2010) 23–229.
[27] Y.G. Chen, K. Tomishige, K. Yokohama, K. Fujimoto, Promoting effect of Pt, Pd and Rh noble metals to the $Ni_{0.03}Mg_{0.97}O$ solid solution catalysts for the reforming of CH_4 with CO_2, Appl. Catal. A: Gen. 165 (1997) 335–347.
[28] C. Crisafulli, S. Scirè, S. Minicò, L. Solarino, Ni–Ru bimetallic catalysts for the CO_2 reforming of methane, Appl. Catal. A: Gen. 225 (2002) 1–9.
[29] K. Takanabe, K.I. Nagaoka, K. Aika, Improved resistance against coke deposition of titania supported cobalt and nickel bimetallic catalysts for carbon dioxide reforming of methane, Catal. Lett. 102 (2005) 153–157.
[30] J. Zhang, H. Wang, A.K. Dalai, Development of stable bimetallic catalysts for carbon dioxide reforming of methane, J. Catal. 249 (2007) 300–310.
[31] J. Kašpar, P. Fornasiero, N. Hickey, Automotive catalytic converters: current status and some perspectives, Catal. Today 77 (2003) 419–449.
[32] X. Wang, J.A. Rodriguez, J.C. Hanson, D. Gamarra, A. Martınez-Arias, M. Fernandez-Garcıa, Ceria-based catalysts for the production of H_2 through the

water–gas-shift reaction: time-resolved XRD and XAFS studies, Top. Catal. 49 (2008) 81–88.
[33] C. Liang, Z. Ma, H. Lin, L. Ding, J. Qiu, W. Frandsen, D. Su, Template preparation of nanoscale $Ce_xFe_{1-x}O_2$ solid solutions and their catalytic properties for ethanol steam reforming, J. Mater. Chem. 19 (2009) 1417–1424.
[34] C. Shi, Y. Ji, U.M. Graham, G. Jacobs, M. Crocker, Z. Zhang, Y. Wan, T.J. Toops, NO_x storage and reduction properties of model ceria-based lean NO_x trap catalysts, Appl. Catal. B: Environ. 119–120 (2012) 183–196.
[35] S.K. Meher, G.R. Rao, Tuning, via counter anions, the morphology and catalytic activity of CeO_2 prepared under mild conditions, J. Colloid Interface Sci. 373 (1) (2012) 46–56.
[36] H. Wu, L. Wang, Shape effect of microstructured CeO_2 with various morphologies on CO catalytic oxidation, Catal. Commun. 12 (2011) 1374–1379.
[37] Tana, M. Zhang, J. Li, H. Li, Y. Li, W. Shen, Morphology-dependent redox and catalytic properties of CeO_2 nanostructures: nanowires, nanorods and nanoparticles, Catal. Today 148 (2009) 179–183.
[38] F. Sadi, D. Duprez, F. Gérard, A. Miloudi, Hydrogen formation in the reaction of steam with Rh/CeO_2 catalysts: a tool for characterising reduced centres of ceria, J. Catal. 213 (2) (2003) 226–234.
[39] A.B. Kehoe, D.O. Scanlon, G.W. Watson, Role of lattice distortions in the oxygen storage capacity of divalently doped CeO_2, Chem. Mater. 23 (2011) 4464–4468.
[40] N. Laosiripojana, W. Sutthisripok, S. Assabumrungrat, Synthesis gas production from dry reforming of methane over CeO_2 doped Ni/Al_2O_3: influence of the doping ceria on the resistance toward carbon formation, Chem. Eng. J. 112 (2005) 13–22.
[41] C.E. Daza, A. Kiennemann, S. Moreno, R. Molina, Dry reforming of methane using Ni–Ce catalysts supported on a modified mineral clay, Appl. Catal. A: Gen. 364 (2009) 65–74.
[42] S. Wang, G.Q.M. Lu, Role of CeO_2 in $Ni/CeO_2–Al_2O_3$ catalysts for carbon dioxide reforming of methane, Appl. Catal. B: Environ. 19 (1998) 267–277.
[43] K. Asami, X. Li, K. Fujimoto, Y. Koyama, A. Sakurama, N. Kometani, Y. Yonezawa, CO_2 reforming of CH_4 over ceria-supported metal catalysts, Catal. Today 84 (2003) 27–31.
[44] V.M. Gonzalez-Delacruz, F. Ternero, R. Pereniguez, A. Caballero, J.P. Holgado, Study of nanostructured Ni/CeO_2 catalysts prepared by combustion synthesis in dry reforming of methane, Appl. Catal. A: Gen. 384 (2010) 1–9.
[45] Z. Wang, X. Shao, A. Larcher, K. Xie, D. Dong, C.-Z. Li, A study on carbon formation over fibrous NiO/CeO_2 nanocatalysts during dry reforming of methane, Catal. Today 216 (2013) 44–49.
[46] A.P.S. Peres, A.C. Lima, B.S. Barros, D.M.A. Melo, Synthesis and characterization of $NiCo_2O_4$ spinel using gelatin as an organic precursor, Mater. Lett. 89 (2012) 36–39.
[47] P. Bharali, G. Thrimurthulu, L. Katta, B.M. Reddy, Preparation of highly dispersed and thermally stable nanosized cerium–hafnium solid solutions over silica surface: structural and catalytic evaluation, J. Ind. Eng. Chem. 18 (2012) 1128–1135.
[48] F. Giordano, A. Trovarelli, C. de Leitenburg, M. Giona, A model for the temperature-programmed reduction of low and high surface area ceria, J. Catal. 193 (2000) 273–282.
[49] G.R. Rao, Influence of metal particles on the reduction properties of ceria-based materials studied by TPR, Bull. Materi. Sci. 22 (2) (1999) 89–94.
[50] S. Xu, X. Yan, X. Wang, Catalytic performances of $NiO–CeO_2$ for the reforming of methane with CO_2 and O_2, Fuel 85 (2006) 2243–2247.
[51] S.M. de Lima, A.M. da Silva, L.O.O. da Costa, U.M. Graham, G. Jacobs, B.H. Davis, L.V. Mattos, F.B. Noronha, Study of catalyst deactivation and reaction mechanism of steam reforming, partial oxidation, and oxidative steam reforming of ethanol over Co/CeO_2catalyst, J. Catal. 268 (2009) 268–281.
[52] L.F. Liotta, G. Di Carlo, G. Pantaleo, A.M. Venezia, G. Deganello, Co_3O_4/CeO_2 composite oxides for methane emissions abatement: relationship between $Co_3O_4–CeO_2$ interaction and catalytic activity, Appl. Catal. B: Environ. 66 (2006) 217–227.
[53] V.M. Gonzalez-delaCruz, R. Pereniguez, F. Ternero, J.P. Holgado, A. Caballero, In situ XAS study of synergic effects on $Ni–Co/ZrO_2$ methane reforming catalysts, J. Phys. Chem. C 116 (2012) 2919–2926.
[54] F.M. Althenayan, S.Y. Foo, E.M. Kennedy, B.Z. Dlugogorski, A.A. Adesina, Bimetallic $Co–Ni/Al_2O_3$ catalyst for propane dry reforming: estimation of reaction metrics from longevity runs, Chem. Eng. Sci. 65 (2010) 66–73.
[55] G. Anandha Babu, G. Ravi, Y. Hayakawa, Surfactant assisted growth and optical studies of $NiCo_2O_4$ nanostructures through microwave heating method, Int. J. Sci. Eng. Appl. (2014) 17–20 (special issue NCRTAM ISSN-2319-7560).
[56] S.Y. Foo, C.K. Cheng, T.-H. Nguyen, A.A. Adesina, Syngas production from CH_4 dry reforming over $Co-Ni/Al_2O_3$ catalyst: coupled reaction-deactivation kinetic analysis and the effect of O_2 co-feeding on H_2:CO ratio, Int. J. Hydrogen Energy 37 (2012) 17019–17026.
[57] V.M. Gonzalez-DelaCruz, J.P. Holgado, R. Pereñíguez, A. Caballero, Morphology changes induced by strong metal–support interaction on a Ni–ceria catalytic system, J. Catal. 257 (2008) 307–314.
[58] K. Takanabe, K. Nagaoka, K. Nariai, K.I. Aika, Titania-supported cobalt and nickel bimetallic catalysts for carbon dioxide reforming of methane, J. Catal. 232 (2005) 268–275.
[59] S. Bernal, J.J. Calvino, M.A. Cauqui, J.M. Gatica, C. López Cartes, J.A. Pérez Omil, J.M. Pintado, Some contributions of electron microscopy to the characterization of the strong metal–support interaction effect, Catal. Today 77 (2003) 385–406.
[60] S. Bernal, J.J. Calvino, M.A. Cauqui, J.A. Perez Omil, J.M. Pintado, J.M. Rodriguez-Izquierdo, Image simulation and experimental HREM study of the metal dispersion in Rh/CeO_2 catalysts: influence of the reduction/reoxidation conditions, Appl. Catal. B: Environ. 16 (1998) 127–138.
[61] D. Uner, N.A. Tapan, I. Ozen, M. Uner, Oxygen adsorption over Pt/TiO_2 catalysts, Appl. Catal. A: Gen. 251 (2) (2003) 225–234.
[62] L. Liu, H. Jiang, H. Liu, H. Li, Recent advances on the catalysts for activation of CO_2 in several typical processes, in: S.L. Suib (Ed.), New and Future Developments in Catalysis: Activation of Carbon Dioxide, Elseviere, 2013, pp. 189–222.
[63] H. Long, Y. Xu, X. Zhang, S. Hu, S. Shang, Y. Yin, X. Dai, Ni–Co/Mg–Al catalyst derived from hydrotalcite-like compound prepared by plasma for dry reforming of methane, J. Energy Chem. 22 (2013) 733–739.
[64] J.H. Lehman, M. Terrones, E. Mansfield, K.E. Hurst, V. Meunier, Evaluating the characteristics of multiwall carbon nanotubes, Carbon 49 (2011) 2581–2602.
[65] D. Bom, R. Andrews, D. Jacques, J. Anthony, B. Chen, M.S. Meier, J.P. Selegue, Thermogravimetric analysis of the oxidation of multiwalled carbon nanotubes: evidence for the role of defect sites in carbon nanotube chemistry, Nano Lett. 2 (6) (2002) 615–619.
[66] D.K. Singh, P.K. Iyer, P.K. Giri, Diameter dependence of oxidative stability in multiwalled carbon nanotubes: role of defects and effect of vacuum annealing, J. Appl. Phys. 108 (2010) 084313.
[67] H. Zhang, Y. Chen, G. Zeng, H. Huang, Z. Xie, X. Jie, The thermal properties of controllable diameter carbon nanotubes synthesized by using AB5 alloy of micrometer magnitude as catalyst, Mater. Sci. Eng. A 464 (2007) 17–22.
[68] D.Y. Kim, Y.S. Yun, S.M. Kwon, H.J. Jin, Preparation of aspect ratio-controlled carbon nanotubes, Mol. Cryst. Liq. Cryst. 510 (2009) 79–86.
[69] H. Li, N. Zhao, C. He, C. Shi, X. Du, J. Li, Thermogravimetric analysis and TEM characterization of the oxidation and defect sites of carbon nanotubes synthesized by CVD of methane, Mater. Sci. Eng. A 473 (2008) 355–359.
[70] G.S.B. McKee, C.P. Deck, K.S. Vecchio, Dimensional control of multi-walled carbon nanotubes in floating-catalyst CVD synthesis, Carbon 47 (2009) 2085–2094.